



# Sedimentation and particle dynamics in the seasonal ice zone of the Barents Sea

Kanchan Maiti <sup>a,c</sup>, JoLynn Carroll <sup>b,\*</sup>, Claudia R. Benitez-Nelson <sup>a</sup>

<sup>a</sup> Department of Geological Sciences, University of South Carolina, Columbia, SC, USA

<sup>b</sup> Akvaplan-niva AS, Polar Environmental Center, Tromsø, Norway

<sup>c</sup> Woods Hole Oceanographic Institution, Woods Hole MA, 02543, USA

## ARTICLE INFO

### Article history:

Received 22 September 2008

Received in revised form 21 May 2009

Accepted 11 September 2009

Available online 23 September 2009

### Keywords:

Radioisotopes

Sedimentation

Bioturbation

Seasonal ice zone

Barents Sea

## ABSTRACT

The Barents Sea seasonal ice zone (SIZ) is one of the most dynamic areas in the world ocean. This biologically productive area undergoes extreme intra- and inter-annual variabilities in sea ice and water mass transport properties. Here, we investigate seafloor burial processes in three regions of the SIZ with different ice-cover frequencies: predominantly open water (POW), marginally ice-covered (MIC), and predominantly ice-covered (PIC) with approximately 0, 10 and 50% sea ice cover, respectively, in 2002–2003. Down-core sediment profiles of the radionuclides <sup>234</sup>Th, <sup>210</sup>Pb, and <sup>137</sup>Cs, along with sediment carbon, nitrogen and phosphorus concentrations are examined in two to three cores from each region. Sedimentation rates and velocities using <sup>210</sup>Pb<sub>ex</sub> (excess <sup>210</sup>Pb) profiles and assuming negligible mixing below a surface mixed layer are relatively uniform throughout the study area, averaging  $558 \pm 154 \text{ g m}^{-2} \text{ y}^{-1}$  and  $1.1 \pm 0.4 \text{ mm y}^{-1}$  ( $n=7$ ). These sedimentation velocities are confirmed using <sup>137</sup>Cs ( $1.0 \pm 0.4 \text{ mm y}^{-1}$ ,  $n=7$ ). <sup>234</sup>Th<sub>ex</sub> (excess <sup>234</sup>Th) derived bioturbation rates are positively correlated with number of benthic individuals per  $0.5 \text{ m}^2$  ( $R^2=0.83$ ) and exhibit a pattern of higher rates in the MIC ( $14.5 \pm 2.1 \text{ cm}^{-2} \text{ y}^{-1}$ ) relative to both the POW ( $6.3 \pm 2.2 \text{ cm}^{-2} \text{ y}^{-1}$ ) and PIC ( $5.3 \pm 1.2 \text{ cm}^{-2} \text{ y}^{-1}$ ) ( $p<0.01$ ). <sup>234</sup>Th<sub>ex</sub> inventories are also significantly higher ( $p=0.026$ ) within the MIC, while both <sup>210</sup>Pb<sub>ex</sub> and <sup>137</sup>Cs sediment inventories are more regionally uniform. Furthermore, organic carbon ( $C_{\text{org}}$ ) and total nitrogen ( $N_{\text{tot}}$ ) concentrations are relatively high in both the MIC and PIC compared to POW. For this limited data set, higher bioturbation rate coefficients and higher <sup>234</sup>Th<sub>ex</sub> sediment inventories in the MIC relative to the other sampled regions, suggest that the MIC exhibits a greater predominance of marine versus terrestrial sediment sources that support enhanced scavenging and benthic biological activity. These results suggest that a climate-driven northward shift in sea ice will result in a corresponding shift in benthic communities that currently depend upon surface derived fluxes of organic matter associated with the present-day location of the ice edge in the Barents Sea.

© 2009 Elsevier B.V. All rights reserved.

## 1. Introduction

The Barents Sea is one of the most productive of the Arctic seas with an estimated average annual primary production of  $90 \text{ gCm}^{-2} \text{ y}^{-1}$  (Wassmann et al., 2006, 2008). A relatively high proportion (~47%) of the sediment burial flux is derived from marine rather than terrestrial sources (Stein and Macdonald, 2004). Depending on the water mass characteristics and physical regimes, between 48 and 96% of primary production in the Barents Sea is estimated to reach the seafloor (Wassmann, 1991; Wassmann and Slagstad, 1993; Wassmann et al., 1999; Carmack and Wassman, 2006). Primary production patterns are strongly correlated with changes in the spatial distribution of sea ice in the Barents Sea. As the seasonal ice zone (SIZ) retreats, pulses of food for higher trophic levels become available to both pelagic and benthic communities (Wassmann et al., 2006). The close relationship between the structure and function of benthic communities and the overlying

primary productivity has been well demonstrated throughout this region (Piepenburg et al., 1995; Renaud et al., 2008; Carroll et al., 2008a).

Recent studies suggest tight pelagic–benthic coupling within the relatively deep (~200–300 m) northwestern margin of the Barents Sea (Tamelander et al., 2006; Renaud et al., 2008; Morata and Renaud, 2008; Carroll et al., 2008a), similar to the relatively shallow (~30–60 m) regions of the Chukchi Sea (Dunton et al., 2005; Grebmeier et al., 2006). Carroll et al. (2008a) showed that Barents Sea benthic communities are food-limited and hence dependent on episodic delivery of organic matter from the water column. As benthic organisms respond to peaks in food supply, there may be an associated increase in intensity and depth of biological mixing in surface sediment deposits.

Sea ice is susceptible to changes in long-term average temperatures and shifts in atmospheric circulation (Polyakov et al., 2005; Deser and Teng, 2008). Over the past 100 years, sea ice extent in the Arctic has diminished by approximately 12 and 40% for April and August, respectively (Vinje, 2001) and the rate of sea ice decline in recent years has accelerated (Serreze et al., 2003; Stroeve et al., 2007; Comiso et al., 2008). Reduced sea ice cover during summer may change the

\* Corresponding author.

E-mail address: [jc@akvaplan.niva.no](mailto:jc@akvaplan.niva.no) (J. Carroll).

temporal and spatial extent of pelagic primary production that may lead to a shift in primary energy pathways between pelagic and benthic food webs (Carroll and Carroll, 2003; Renaud et al., 2008). Climate-related and anthropogenically-induced changes in the location of the SIZ are thus likely to have far reaching consequences on the structure and function of Arctic marine ecosystems (Carroll and Carroll, 2003; Grebmeier et al., 2006; Wassmann et al., 2008). It is therefore essential to understand how such changes might affect primary production, sedimentation and pelagic–benthic coupling processes in the Barents Sea SIZ.

There is currently little information on modern sediment accumulation processes and carbon burial rates in the Barents Sea. Sediment deposits for this region consist of fine-grained clays and silts interspersed with layers of sand, representing typical marine, hemipelagic sedimentation (Ivanova et al., 2002). Particle-associated radioisotopes are powerful tools to examine modern sedimentary processes and are often employed as tracers of particle reworking, sedimentation rates, and sediment transport processes (Krishnaswami et al., 1980; Huh et al., 1997; Smoak et al., 2000; Carroll and Lerche, 2003; Smith et al., 2003; Meysman et al., 2005). Briefly  $^{210}\text{Pb}$  ( $t_{1/2} = 22.3$  years) produced from the decay of atmospheric  $^{222}\text{Rn}$  enters the oceans predominantly via atmospheric deposition to the ocean surface (Turekian et al., 1977) where it quickly adsorbs to sinking particles and is transported to underlying sediments. This  $^{210}\text{Pb}$  is in excess of that supported by  $^{222}\text{Rn}$  decay within the sediments and provides information regarding particle reworking and sedimentation rates over time-scales of  $\sim 100$  years (Robbins, 1978; Cochran, 1992; Appleby and Oldfield, 1992; Smoak et al., 2000).  $^{234}\text{Th}$  ( $t_{1/2} = 24.1$  days) is another particle reactive radionuclide derived from the decay of its conservative and soluble parent  $^{238}\text{U}$  in the water column. Once produced,  $^{234}\text{Th}$  rapidly adsorbs to sinking particles and reaches the seafloor, where it is in excess of that produced from  $^{238}\text{U}$  decay within the sediments. Due to its relatively short half-life, the presence of excess  $^{234}\text{Th}$  in surficial sediments is often interpreted as an indicator of short-term bioturbation rates or rapid deposition events (Crusius et al., 2004; Aller and Cochran, 1976) over time-scales of few months ( $\sim 5$  months). Given the fact that burial flux in this region is predominantly derived from marine biological production, most of which is consumed by food-limited benthic communities during the summer months, bioturbation most likely dominates burial.

In this study, we investigate sediment depth profiles of the radionuclides,  $^{210}\text{Pb}$ ,  $^{137}\text{C}$ , and  $^{234}\text{Th}$  together with sedimentary constituents, organic carbon, nitrogen and phosphorus in sediment cores collected from the central Barents Sea during summer 2003. Using these tracers, we are able to evaluate seasonal bioturbation rates associated with benthic activity in context with decadal-scale sediment burial. Our purpose is to assess whether sedimentation and post-depositional biological mixing processes relate to sea ice cover and hence, higher primary production within the SIZ.

## 2. Materials and methods

### 2.1. Collection

This study was carried out in the SIZ of the central Barents Sea between  $73^\circ$  and  $79^\circ\text{N}$  (Fig. 1). Sediment cores were collected at nine stations from the R/V *Ivan Petrov* in August 2003. Stations were located along three north–south transects covering areas of predominantly open water (POW), marginally ice-covered (MIC), and predominantly ice-covered (PIC) (Table 1). These areas represent regions of the Barents Sea with annual sea ice cover of approximately 0% (POW), 10% (MIC) and 50% (PIC) based both on ice-cover statistics for 2000–2003 as well as long-term sea-ice data from 1981–2000 (Keup-Thiel et al., 2006). Sediments were collected using a 0.25 m<sup>2</sup> box corer. A box corer may lead to the loss of surface sediments if not

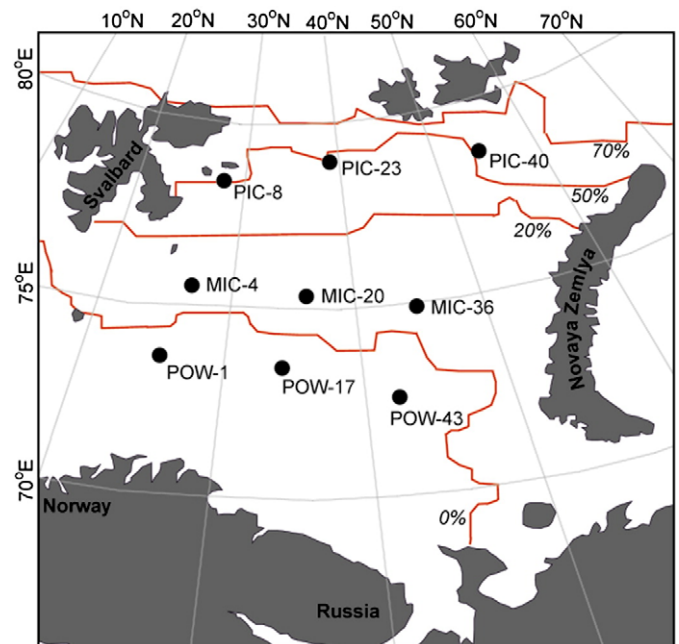


Fig. 1. The Barents Sea SIZ with sampling locations. The red lines show the average percent ice cover over past two decades (ice data from Keup-Thiel et al., 2006). (For interpretation of the references to color in this figure legend, the reader is referred to the web version of this article.)

deployed carefully. During sediment collection, three cores exhibited evidence of surface layer disturbance and therefore were discarded. The presence of large concentrations of benthic pigments ( $2\text{--}10 \mu\text{g g}^{-1}$  dry weight) in the surface layer of retrieved cores (Cochrane et al., 2009) indicates recent settlement of fresh material, which would not be present if the surface layers had been lost. However, we cannot completely rule out the loss of some surface material, which would affect the accuracy of our derived  $^{234}\text{Th}$  mixing rates. For radioisotope analyses, a 140 mm diameter sub-core was collected from each box core by carefully inserting a sharpened PVC tube. Cores were kept vertical and frozen until processed, usually within 1 h of collection. Sediments were extruded upward using a vertical rack and a piston inserted at the bottom of the core barrel. Sediment cores were sectioned into 0.5 cm intervals over the upper 5 cm, 1 cm intervals over the upper 5–10 cm and at 2 cm intervals below a depth of 10 cm. The material in direct contact with the barrel ( $\sim 1$  cm from outer surface) was trimmed and discarded to avoid contamination and smearing artifacts. A homogenized sub-sample from each core section was then used to fill small glass vials of known volumes. The sub-samples were stored refrigerated. Sample materials were returned to the University of South Carolina Radiobiogeochemistry Laboratory for processing. Sediments in the glass vials were weighed and dried at  $60^\circ\text{C}$  in a radiant oven with filtered air. After drying, the samples were reweighed and the data were used to calculate sediment porosities and densities. The samples were subsequently disaggregated and ground with an agate mortar and pestle.

### 2.2. Porosity and sediment density values

Sediment porosity values (Fig. 2) were determined using a wet–dry method [(water weight/dry sediment weight  $\times 100$ ). Dry sediment density ( $\text{g cm}^{-3}$ ) was derived according to the relation  $d_{\text{sd}} = (\text{dry sediment weight in the vial}) / (\text{dry sediment volume})$ . Dry sediment volume was derived as the difference between the vial volume and volume of sediment water content [water volume = (weight of vial with un-dried sample – weight of vial with dried sample) / density of seawater]. All measurements include salt corrections with errors in

**Table 1**  
Station information: location, water depth, pelite fraction (<0.063 mm), radionuclide inventories, average  $C_{org}$ ,  $N_{tot}$ ,  $P_{org}$ ,  $C_{org}/N_{tot}$  in surface mixed layer, mixed layer depth, surface layer mixing coefficients derived from  $^{210}Pb_{ex}$  ( $D_{BMAX}$ ) and  $^{234}Th_{ex}$  ( $D_B$ ) depth profiles.

Station	Lat Long	Depth (m)	Ice cover <sup>a</sup> (%)	ppb (gC m <sup>-2</sup> y <sup>-1</sup> )	Pelite surface	$^{210}Pb_{ex}$ inventory (Bq m <sup>-2</sup> )	$^{137}Cs$ inventory (Bq m <sup>-2</sup> )	$^{234}Th$ inventory (Bq m <sup>-2</sup> )	$C_{org}$ %	$N_{org}$ %	Mixed depth <sup>c</sup> (cm)	$^{234}Th_{ex} D_B$ (cm <sup>2</sup> y <sup>-1</sup> )	$^{210}Pb_{ex} D_{BMAX}$ (cm <sup>2</sup> y <sup>-1</sup> )	Benthic individuals <sup>a</sup> (no. per 0.5 m <sup>2</sup> )
POW-1	73°08' 25°38'	425	0	134	89%	9.01	269	57	1.4 ± 0.1	0.18 ± 0.01	4.0	8.8 ± 2.8 $R^2 = 0.91$	0.5 ± 0.2 $R^2 = 0.85$	1200
POW-17	73°03' 35°35'	224	0	90	54%	12.47	205	140	1.4 ± 0.2	0.16 ± 0.01	5.1	4.6 ± 1.7 $R^2 = 0.94$	0.4 ± 0.1 $R^2 = 0.99$	2985
POW-43	72°31' 45°42'	284	0	75	53%	8.92	190	73	-	-	22	5.4 ± 1.7 $R^2 = 0.94$	-	586
MIC-4	75°02' 26°13'	218	6	101	62%	16.95	223	146	2.1 ± 0.2	0.30 ± 0.02	5.3	-	-	1828
MIC-20	75°19' 37°33'	169	11	61	36%	11.03	345	204	-	-	14	16.4 ± 6 $R^2 = 0.90$	-	1837
MIC-36	74°58' 47°00'	243	6	40	51%	14.49	406	223	1.8 ± 0.1	0.23 ± 0.02	10	13.1 ± 4 $R^2 = 0.93$	2.7 ± 0.4 $R^2 = 0.94$	1921
PIC-8	77°59' 26°50'	136	55	56	77%	6.14	331	48	1.6 ± 0.1	0.19 ± 0.01	6.3	4.0 ± 1.4 $R^2 = 0.91$	1.0 ± 0.2 $R^2 = 0.90$	660
PIC-23	77°29' 39°26'	217	43	30	89%	3.17	94	85	-	-	5.4	5.5 ± 0.7 $R^2 = 0.99$	1.5 ± 0.8 $R^2 = 0.66$	453
PIC-40	78°14' 53°07'	305	51	17	69%	6.87	293	114	1.6 ± 0.1	0.20 ± 0.01	6.7	6.3 ± 1.4 $R^2 = 0.99$	0.7 ± 0.2 $R^2 = 0.90$	203

Model equations and assumptions are given in the text.

<sup>a</sup> Benthic individuals and ice cover (% average 2000–2003) reported in Cochrane et al. (2009).

<sup>b</sup> PP modeled integrated water column productivity (see text for details).

<sup>c</sup> The mixed depth corresponds to the porosity-corrected depth profiles shown in Fig. 4.

porosity representing the standard deviation of the mean porosity for two adjacent depth measurements.

### 2.3. Radionuclide analysis

Aliquots of finely ground dry sediments (5–9 g) were placed into counting vials of known geometry and measured for  $^{210}Pb$ ,  $^{234}Th$ ,  $^{226}Ra$  and  $^{137}Cs$  by direct gamma counting using two high purity germanium well detectors. The detector efficiencies were determined using EPA standard sand spiked with a National Institute of Standards and Technology (NIST) traceable mixed gamma liquid standard from Analytix™, Inc. No correction for self-absorption of the low energy gamma peaks of  $^{234}Th$  and  $^{210}Pb$  was needed since the sample sediment was, within error, close to the density of the spiked sand used to calibrate the detectors. The gamma-ray spectra were then analyzed for peak area and position using the computer program HYPERMET, a reiterative parabolic curve fitting procedure (Phillips and Marlow, 1976). All activities were corrected for decay to the midpoint of sample collection.  $^{210}Pb$  was measured by its emission at 46.5 keV and  $^{226}Ra$  by the 351 keV emission of its daughter isotope  $^{214}Pb$ . Unsupported  $^{210}Pb$  ( $^{210}Pb_{ex}$ ) was calculated as the difference between the measured total  $^{210}Pb$  at 46.5 keV and the estimate of the supported  $^{210}Pb$  activity given by its parent nuclide at 351 keV ( $^{210}Pb_{ex} = ^{210}Pb_{tot} - ^{214}Pb$ ). Both supported and total  $^{210}Pb$  measurements were conducted at least 25 days after initial sample collection.  $^{234}Th$  activity was measured by its emission at 63.5 keV and the supported  $^{234}Th$  activity was measured by recounting the samples more than 5 months (6 half-lives) after collection ( $^{234}Th_{ex} = ^{234}Th_{initial} - ^{234}Th_{final}$ ). The  $^{210}Pb_{ex}$  and  $^{234}Th_{ex}$  profiles used to calculate sedimentation, mixing rates and inventories extend from the surface layer to the deepest sampling interval where excess activities were detected. Below these layers the  $^{210}Pb_{ex}$  and  $^{234}Th_{ex}$  activities are  $\leq 0$ , within the propagated error.  $^{137}Cs$  activity was measured by its emissions at 661 keV. Errors represent counting statistics and the error associated with the HYPERMET curve fitting routine.

### 2.4. Elemental analysis

Total carbon ( $C_{tot}$ ), organic carbon ( $C_{org}$ ) and total nitrogen ( $N_{tot}$ ) were measured using a Perkin-Elmer 2400 CHN elemental analyzer. For  $C_{org}$ , samples were weighed into silver capsules and acidified with concentrated HCl under vacuum for 30h. The samples were then dried in an oven at 50 °C, folded and analyzed (Hedges and Stern, 1984). Approximately 20% of the samples were run in duplicate and duplicates agreed to <5% of each other. The inorganic fraction of nitrogen was assumed to be negligible because the organic carbon content is ~1%.

Particulate inorganic phosphorus (IP) and total particulate phosphorus (TP) content were determined following the method outlined by Aspila et al. (1976). Particulate organic phosphorus (OP) was calculated by difference ( $OP = TP - IP$ ). It is important to note here that the distinction between IP and OP is operationally defined. Thus, it is possible that some of the 'inorganic' particulate P fraction contains labile organic compounds and vice versa. A standard reference material, NIST 1573a (tomato leaves) was run with each sample set to evaluate total P recovery and reproducibility between runs. Approximately 20% of the samples were run in duplicate and duplicates agreed to <5% of each other.

### 2.5. $^{210}Pb$ modeling approach

The general equation describing steady-state conservation for a radiotracer subjected to advective supply and/or biotransformation in sediments (Krishnaswami et al., 1980; DeMaster et al., 1985; Cochran, 1992; Meysman et al., 2005 and references therein) is:

$$\frac{\delta}{\delta z} \left[ \phi^s D_B \frac{\delta A^s}{\delta z} \right] - \frac{F_{sed}^s \delta A^s}{\rho^s \delta z} - \phi^s \lambda A^s = 0 \quad (1)$$

where  $A^s$  is tracer activity,  $z$  is depth (cm),  $\rho^s$  is the density of the solid phase ( $\text{g cm}^{-3}$ ),  $\varphi^s$  is the solid volume fraction,  $D_B$  ( $\text{cm}^2 \text{y}^{-1}$ ) is the biodiffusion coefficient that characterizes mixing intensity on a depth scale,  $F_{\text{sed}}^s$  is the sedimentation rate or constant flux of solid sediment arriving at the seafloor ( $\text{g cm}^{-2} \text{y}^{-1}$ ) and  $\lambda$  is the radioactive decay constant ( $\lambda^{210\text{Pb}} = 0.031 \text{y}^{-1}$ ).

Although irrelevant for the biodiffusion model applied in the present investigation (Eq. (1)), porosity profiles are helpful toward assessing the influence of biology on porosity (Fig. 2). With the exception of Station POW-17, many stations exhibit clearly differentiated depth intervals of  $^{210}\text{Pb}_{\text{ex}}$  that are characterized by relatively

uniform sediment porosities; an indication that surface sediment disturbance reflects interphase biological mixing (Meysman et al., 2005).

Applying the assumption of steady-state porosity to the general form of Eq. (1), we first correct our sediment depths for the influence of sediment compaction in accordance with the relation:

$$\phi_z = (\phi_0 - \phi_\infty)e^{-\alpha z} + \phi_\infty, \quad (2)$$

(Athy, 1930) where,  $\phi_0$  is the porosity at the sediment surface,  $\phi_\infty$  is the porosity at final compaction ( $z = \infty$ ), and  $\alpha$  is the coefficient of the

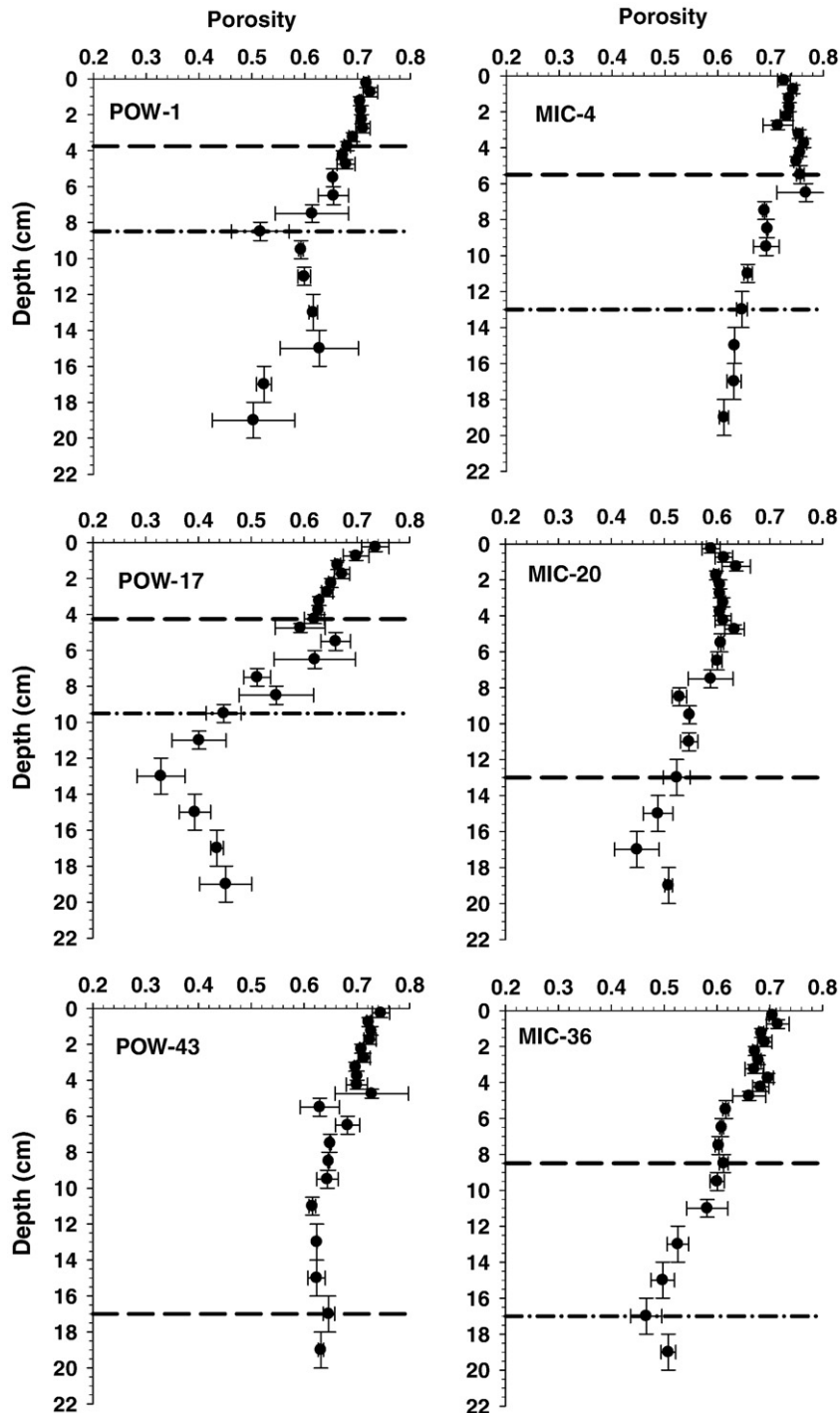


Fig. 2. Changes in sediment porosity with sediment depth ( $z$ ). The depth of  $^{210}\text{Pb}_{\text{ex}}$  penetration (dash-dotted line) and surface mixed layer ( $z^*$ , dashed line) are indicated.

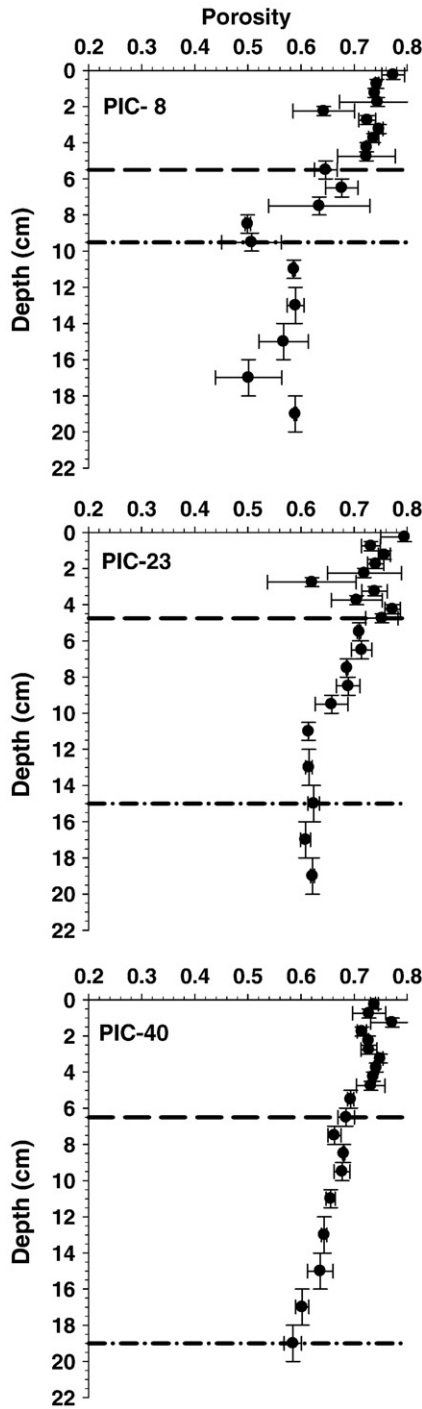


Fig. 2 (continued).

porosity–depth relationship (Eq. (2)). The depth of sediments without compaction ( $z'$ ) is then:

$$z' = z + \int_0^z \frac{\phi_0 - \phi_z}{1 - \phi_0} dz. \quad (3)$$

For each station, de-compacted core depths were derived using a simple approximation to Eq. (3) whereby,

$$z = \sum h', \text{ and } h' = h + \frac{\phi_0 - \phi_z}{1 - \phi_0} h, \quad (4)$$

with  $h$  (cm) as the thickness of a sediment section with compaction and  $h'$  is the corrected (de-compacted) section thickness (Matsumoto, 1975).

Assuming that a given  $^{210}\text{Pb}_{\text{ex}}$  concentration profile is in steady-state, the relationship between advective velocity ( $\omega$ ) and the biodiffusive mixing coefficient ( $D_B$ ) is described as (Smith et al., 1986/87, 1995; Carroll et al., 2008b):

$$A = A_0 \exp \left[ \left( \frac{\omega - \sqrt{\omega^2 + 4D_B\lambda}}{2D_B} \right) z' \right] \quad (5)$$

where  $A_0$  is the  $^{210}\text{Pb}_{\text{ex}}$  activity at  $z' = 0$  and  $A$  is the activity at depth  $z'$ . As shown by Meysman et al. (2005) for the case of a steady-state tracer concentration and porosity, sedimentation velocity ( $\omega_{\text{sed}}$ ) and sediment accumulation velocity ( $\omega_{\text{acc}}$ ) are equal and related to the sedimentation rate  $F_{\text{sed}}^s$  as,

$$\omega = \omega_{\text{sed}} = \omega_{\text{acc}} = \frac{1}{\rho^s \phi_{\text{fix}}^s} F_{\text{sed}}^s. \quad (6)$$

Hence the down-core profile of  $^{210}\text{Pb}_{\text{ex}}$  is described as a combination of biodiffusive and advective transport. As a further simplification, we invoke a two-layer (surface and deep) system. The mixed depth ( $z^*$ ) is distinguished by a change in the slope of the natural log transformed  $^{210}\text{Pb}_{\text{ex}}$  versus sediment depth profile (dashed line in Fig. 3). The suggestion of interphase biological sediment reworking from the observed porosity profiles lends support to the application of this simplified modeling approach. We then derive end-member solutions to Eq. (5) assuming mixing only in the surface layer ( $\omega \neq 0$ ;  $z' < z^*$ ) and sedimentation only in the deep layer ( $D_B = 0$ ;  $z' > z^*$ ). In accordance with the assumption of negligible sedimentation in the surface layer (i.e.  $\omega = 0$  for  $z' < z^*$  in Eq. (5)), the derived surface layer biodiffusive mixing coefficients represent maximum values ( $D_{\text{BMAX}}$ ). The solution to Eq. (5) for  $\omega = 0$  ( $z' < z^*$ ) is:

$$A = A_0 \exp \left[ \sqrt{\frac{\lambda}{D_{\text{BMAX}}}} z' \right]. \quad (7)$$

Determining the slope  $\sqrt{\left(\frac{\lambda}{D_{\text{BMAX}}}\right)}$  of the natural log transformed  $^{210}\text{Pb}_{\text{ex}}$  profile versus de-compacted sediment depth ( $z'$ ) yields a coefficient of biodiffusional mixing ( $D_{\text{BMAX}}$ ).

Similarly, for the assumption of negligible mixing in the deep layer ( $D_B = 0$ ;  $z' > z^*$ ), Eq. (7) becomes,

$$A = A_0 \exp \left[ -\frac{\lambda}{\omega} z' \right]. \quad (8)$$

Sedimentation velocity is then derived from the linear slope ( $\frac{\lambda}{\omega}$ ) term of the natural log transformed  $^{210}\text{Pb}_{\text{ex}}$  profile versus compaction-corrected depth ( $z'$ ). Sediment velocities and mixing rates are reported in units of  $\text{mm y}^{-1}$  and  $\text{cm}^2 \text{y}^{-1}$ , respectively, with associated errors derived from the standard error of the linear slope value of the natural log transformed  $^{210}\text{Pb}_{\text{ex}}$  profiles (Tables 1 and 2). For comparison, we calculate  $\omega$  values assuming negligible sediment mixing at each station, i.e. ( $D_B = 0$ ;  $z^* = 0$ ). Sediment velocities are generally higher, sometimes by as much as ~50% (Table 2). Conversely, if our chosen  $z^*$  estimates are conservative then as  $z^* \rightarrow z_{\text{MAX}}$ ,  $\omega \rightarrow 0$ , where  $z_{\text{MAX}}$  is the sediment depth at the bottom of the  $^{210}\text{Pb}_{\text{ex}}$  profile. Indeed at two of the nine sampling sites (MIC-20 and POW-43) the  $^{210}\text{Pb}_{\text{ex}}$  depth profiles were well mixed and therefore Eq. (5) was not applied to the  $^{210}\text{Pb}_{\text{ex}}$  profiles from these two stations. In addition, a biodiffusive mixing coefficient could also not be determined for MIC-4 due to the sharp gradient in  $^{210}\text{Pb}_{\text{ex}}$  observed.

2.6. <sup>234</sup>Th modeling approach

The governing assumptions and equations used to describe <sup>210</sup>Pb<sub>ex</sub> profiles in surface sediments are equally valid for <sup>234</sup>Th<sub>ex</sub> ( $\lambda = 11.363 \text{ y}^{-1}$ ). The half-life of <sup>234</sup>Th is short compared to previously reported sedimentation velocities (Zaborska et al., 2008), thus  $\omega$  in Eq. (5) may be assumed negligible ( $\omega = 0$ , see Sediment

mixing). Sediment porosity is relatively uniform above the depth of <sup>234</sup>Th<sub>ex</sub> penetration (<sup>234</sup>Th<sub>ex</sub> > 0 Bq/kg), which corresponds to 3–4 cm below the sediment–water interface. This eliminates the need to correct sediment depths for the influence of compaction. Hence mixing coefficients,  $D_B$ , are derived directly from the slope  $\sqrt{\left(\frac{\Delta}{D_B}\right)}$  of the natural log transformed <sup>234</sup>Th<sub>ex</sub> versus depth (z) profiles (Fig. 4).

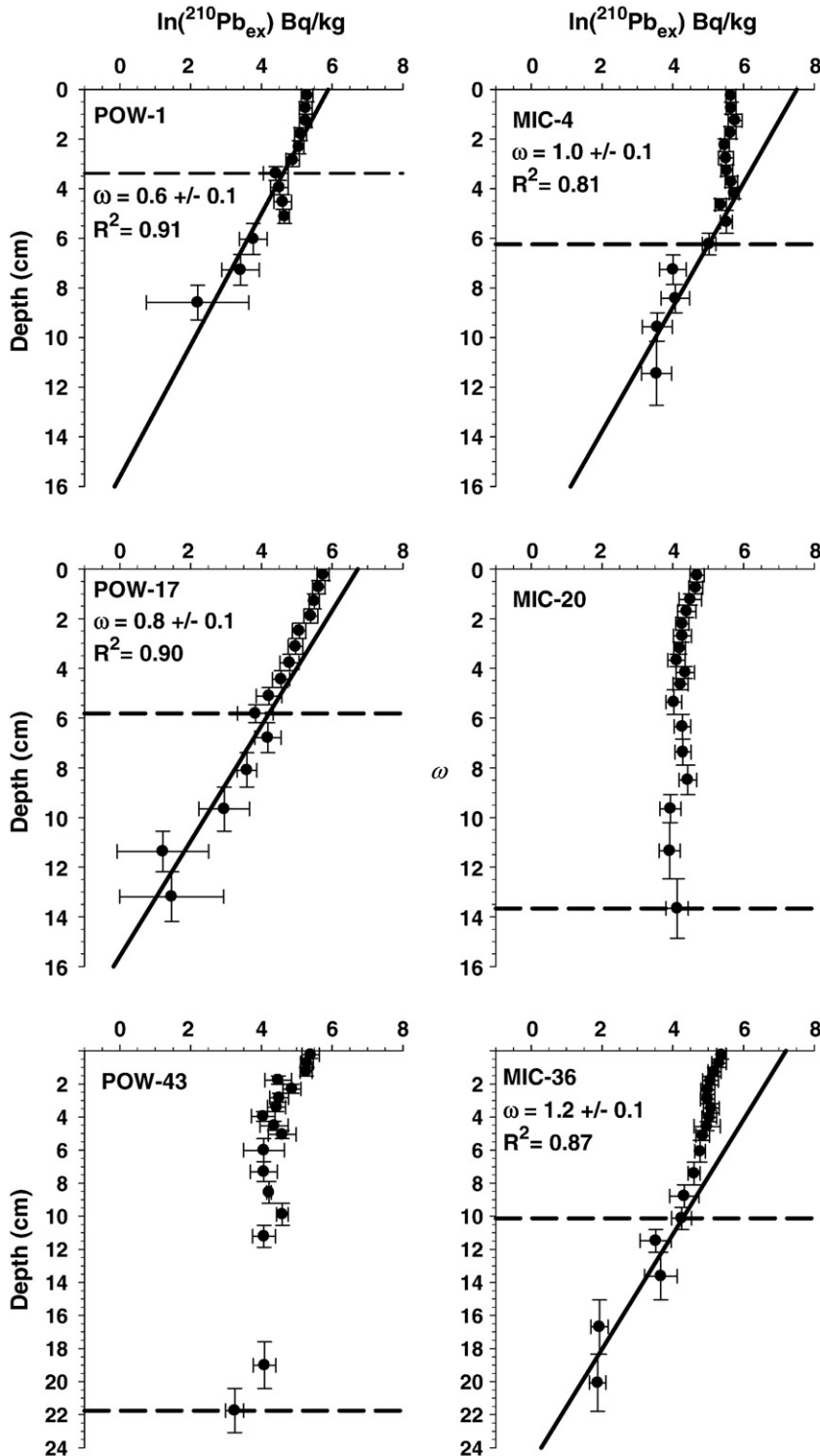


Fig. 3. Profiles of <sup>210</sup>Pb<sub>ex</sub> versus de-compacted sediment depth (z'). The linear regression best fit to the <sup>210</sup>Pb<sub>ex</sub> versus depth z' over the interval (z' > z\*) is shown (solid line). Sediment velocity values ( $\omega$ ) were derived in accordance with Eq. (8). The surface mixed layer (z\*, dashed line) is shown.

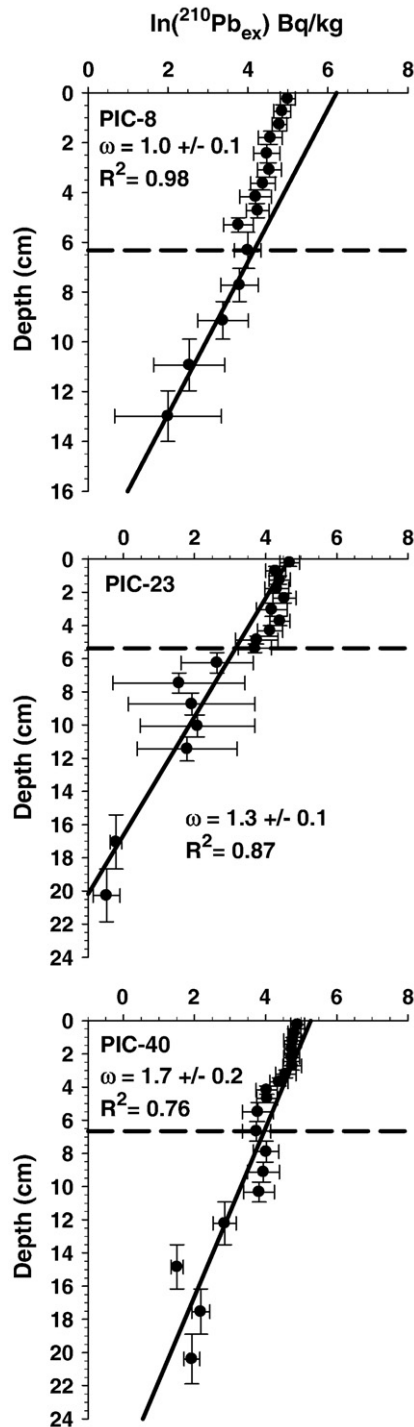


Fig. 3 (continued).

The errors reported for  $^{234}\text{Th}_{\text{ex}}$  mixing rates were derived from the standard error of the linear slope term of the natural log transformed  $^{210}\text{Pb}_{\text{ex}}$  profiles.

### 2.7. $^{137}\text{Cs}$ as a time marker

$^{137}\text{Cs}$  ( $t_{1/2} = 30$  years) is often used in conjunction with  $^{210}\text{Pb}_{\text{ex}}$  as a marker of specific date horizons (Anderson et al., 1988; Ritchie and McHenry, 1990; Appleby, 2001). Significant levels of  $^{137}\text{Cs}$  first appeared in the atmosphere during the 1950s as a result of above ground nuclear testing. Atmospheric  $^{137}\text{Cs}$  concentrations peaked in

1962, with maximum fallout in 1963 (Carter and Moghissii, 1977). Following the Chernobyl Nuclear accident in 1986, the atmospheric concentration of  $^{137}\text{Cs}$  in Europe peaked at approximately 4-times higher than 1963 levels, and lasted for several months (Cambray et al., 1987). These two dates, 1963 and 1987, are commonly applied to peaks in  $^{137}\text{Cs}$  concentration observed in sediments and used as a chronostratigraphic marker (Anderson, et al., 1988; Appleby, 2001; Lima et al., 2005). In spite of the presence of  $^{137}\text{Cs}$  activity in all nine sediment cores, the  $^{137}\text{Cs}$  peak for 1987 was not well defined. Therefore, only the 1963  $^{137}\text{Cs}$  peak is used as a stratigraphic time marker (Fig. 5). A  $^{137}\text{Cs}$  sedimentation velocity was subsequently determined for each station by dividing the depth ( $z'$ ) of the observed 1963  $^{137}\text{Cs}$  peak in each core by 40 years (2003–1963) (Table 2). Two of the nine sampling sites (MIC-20 and POW-43) showed no clear peaks in  $^{137}\text{Cs}$  activity as well as uniform  $^{210}\text{Pb}_{\text{ex}}$  depth profiles. These cores were considered well mixed and therefore, sedimentation rates, were not determined.

### 2.8. Radionuclide inventories

Inventories of  $^{210}\text{Pb}_{\text{ex}}$ ,  $^{234}\text{Th}_{\text{ex}}$ , and  $^{137}\text{Cs}$  are calculated as the cumulative sum of  $^{210}\text{Pb}_{\text{ex}}$  ( $\text{Bq g}^{-1}$ ),  $^{234}\text{Th}_{\text{ex}}$  ( $\text{Bq g}^{-1}$ ) and  $^{137}\text{Cs}$  ( $\text{Bq g}^{-1}$ ) multiplied by cumulative mass of each sediment layer ( $\text{g cm}^{-2}$ ). Radionuclide inventories were quantified from the surface sediment layer down to the depth where the radionuclide activity is below detection.  $^{210}\text{Pb}_{\text{ex}}$  inventories are presented in  $\text{Bq cm}^{-2}$  and  $^{137}\text{Cs}$  and  $^{234}\text{Th}_{\text{ex}}$  inventories in  $\text{Bq m}^{-2}$  (Table 1).

## 3. Results and discussion

### 3.1. Sediment mixing

Due to the strong seasonal nature of productivity and tight coupling between pelagic and benthic ecosystems in the Barents Sea, an increase in intensity and depth of biological mixing in surface sediment deposits may occur in concert with peak biological productivity (spring–summer) at the sea ice margin. The presence of short-lived  $^{234}\text{Th}_{\text{ex}}$  to  $\leq 5$  cm depth in all cores (Fig. 3) indicates a clear signal of recent events at the sediment–water interface; attributable to either rapid deposition or recent post depositional mixing of sediments. Here, we assume that  $^{234}\text{Th}$  reflects bioturbation rather than abiotic mixing or rapid sedimentation. Abiotic mixing is unlikely given the depth of the sediment cores ( $> 130$  m, Table 1), low current velocities at depth in this region (Schauer et al., 2002; Bellec et al., 2008), and the high percentage of fine pelite material ( $< 0.063$  mm) in the sediment core surface layers (Table 1). While rapid deposition can occur, and may have indeed happened for MIC-20 and POW-43, the limited depth penetration of  $^{234}\text{Th}$  in the remaining cores and the rapid decline of  $^{234}\text{Th}$  with depth suggests that mixing is the dominant process (Fig. 4). Excluding Station POW-17, we obtain a positive linear correlation ( $r^2 = 0.83$ ) between  $^{234}\text{Th}$  based mixing rates and the number of benthic individuals measured per  $0.5 \text{ m}^2$ , as reported for all stations in Cochrane et al. (2009) (Fig. 6). This relationship supports our hypothesis that  $^{234}\text{Th}$  based mixing rates are biologically mediated.

Assuming that  $^{234}\text{Th}_{\text{ex}}$  in the upper few centimeters of each core results only from active mixing, biodiffusive mixing coefficients range from  $4.0$  to  $16 \text{ cm}^2 \text{ y}^{-1}$  (Fig. 2, Table 1). We were unable to determine a mixing coefficient at station MIC-4 using the biodiffusion model (Eq. (7)) due to a subsurface peak in  $^{234}\text{Th}$  activity (Fig. 4). This peak may be a result of sediment translocation by selective deposit feeding organisms (Aller and DeMaster, 1984; Miller et al., 2000). Statistical comparison of  $^{234}\text{Th}_{\text{ex}}$   $D_B$  coefficients by ice-cover region for all other stations yielded a significant regional relationship (1-way ANOVA,  $p = 0.006$ ). Mean  $^{234}\text{Th}_{\text{ex}}$   $D_B$  values were significantly higher in the MIC region ( $14.8 \pm 2.1 \text{ cm}^2 \text{ y}^{-1}$ ) when compared to either the PIC

**Table 2**  
Sedimentation velocities ( $\omega$  in units of  $\text{mmy}^{-1}$ ) and sedimentation rates (SR in units of  $\text{g m}^{-2}\text{y}^{-1}$ ) determined for  $^{210}\text{Pb}_{\text{ex}}$  versus porosity-corrected depth.

Station	$\omega$ (below mixed layer)	$\omega$ (whole core)	SR (below mixed layer)	$\omega$ ( $^{137}\text{Cs}$ time marker)
POW-1	$0.6 \pm 0.1$ $R^2 = 0.91$	$0.9 \pm 0.1$ $R^2 = 0.87$	$352 \pm 25$ $R^2 = 0.91$	0.5
POW-17	$0.8 \pm 0.1$ $R^2 = 0.90$	$0.9 \pm 0.1$ $R^2 = 0.95$	$458 \pm 35$ $R^2 = 0.90$	0.8
POW-43	–	–	–	–
MIC-4	$1.0 \pm 0.1$ $R^2 = 0.87$	$1.4 \pm 0.2$ $R^2 = 0.83$	$530 \pm 51$ $R^2 = 0.87$	1.0
MIC-20	–	–	–	–
MIC-36	$1.2 \pm 0.1$ $R^2 = 0.87$	$1.7 \pm 0.1$ $R^2 = 0.92$	$539 \pm 42$ $R^2 = 0.87$	1.6
PIC-8	$1.0 \pm 0.1$ $R^2 = 0.98$	$1.4 \pm 0.1$ $R^2 = 0.95$	$592 \pm 19$ $R^2 = 0.98$	1.1
PIC-23	$1.3 \pm 0.1$ $R^2 = 0.87$	$1.1 \pm 0.1$ $R^2 = 0.93$	$579 \pm 53$ $R^2 = 0.87$	0.9
PIC-40	$1.7 \pm 0.2$ $R^2 = 0.76$	$1.9 \pm 0.2$ $R^2 = 0.89$	$853 \pm 100$ $R^2 = 0.76$	1.4

Sedimentation velocities ( $\omega$ ) are calculated assuming  $D_B = 0$  (whole core) and  $D_B = 0$  (below the surface mixed depth). Mixed depths are reported in Table 1.  $^{137}\text{Cs}$  sedimentation velocities ( $\text{mmy}^{-1}$ ) are based on the depth of the maximum in  $^{137}\text{Cs}$  activity (see Fig. 5), attributed to the 1963 peak in atmospheric fallout from nuclear weapons testing ( $^{137}\text{Cs}$  time marker).

( $5.3 \pm 1.1 \text{ cm}^2\text{y}^{-1}$ ) or POW ( $6.3 \pm 2.2 \text{ cm}^2\text{y}^{-1}$ ) (post hoc Tukey;  $p < 0.01$ ), while PIC and POW means were similar ( $p = 0.81$ ).

Surface layer  $^{210}\text{Pb}_{\text{ex}}$   $D_B$  coefficients are lower than the  $^{234}\text{Th}_{\text{ex}}$   $D_B$  coefficients and there is only a weak linear relationship between  $^{234}\text{Th}_{\text{ex}}$  and  $^{210}\text{Pb}_{\text{ex}}$   $D_B$  coefficients ( $R^2 = 0.5$ ;  $p > 0.05$ ). We do not expect  $D_B$  rates derived from these radionuclides to be similar because different tracers integrate processes over different time-scales (DeMaster et al., 1985; Pope et al., 1996; Renaud et al., 2008).  $^{234}\text{Th}_{\text{ex}}$  rates reflect recent events that have taken place in the most active bioturbation zone of the upper few centimeters of sediment, while  $^{210}\text{Pb}_{\text{ex}}$  rates integrate events recorded within the upper  $\sim 10$  cm of sediment deposits, corresponding to time-scales of years to decades. We therefore hypothesize that the derived  $^{234}\text{Th}_{\text{ex}}$  biological mixing rates provide a snapshot of tight pelagic–benthic coupling associated with melting sea ice in spring and summer 2003 (e.g. see Fig. 6). Sedimentary profiles of  $^{234}\text{Th}$  and  $^{210}\text{Pb}$  from the northwestern Barents Sea also indicated a zone of mixing extending only a few centimeters below the sediment–water interface, and associated rate coefficients ( $^{234}\text{Th} = 1\text{--}12 \text{ cm}^2\text{y}^{-1}$ ;  $^{210}\text{Pb} = 0\text{--}0.2 \text{ cm}^2\text{y}^{-1}$ ) towards the lower range of values reported for most continental shelf seas (e.g. Smith et al., 1995; Soetaert et al., 1996; Gerino et al., 1998; Alperin et al., 1999). Despite the prevalence of surface and subsurface deposit feeding organisms on the shelf (Wassmann et al., 2006; Carroll et al., 2008a), bioturbation in this region leads to low intensity sediment mixing (Carroll et al., 2008b).

### 3.2. Sedimentation rates

$^{210}\text{Pb}_{\text{ex}}$  sedimentation velocities and sedimentation rates, quantified below the zone of active sediment mixing (Table 2), exhibit no distinct spatial pattern of sediment accumulation. These velocities are supported by estimates based on  $^{137}\text{Cs}$  as a time marker for 1963 (Table 2). Similar regional uniformity and absolute magnitude of sedimentation velocities and rates of  $0.7 \pm 0.4 \text{ mmy}^{-1}$  were reported for the northwest Barents Sea (Zaborska et al., 2008; Carroll et al., 2008b). Although large scale shifts in ice cover have remained minimal over the past 20 years (Fig. 1) in the MIC, PIC, and POW, subtle changes in ice cover, sediment focusing and ice-rafted sediments (see Radionuclide inventories), and benthic boundary layer processes operating over the time-scale of detection for  $^{210}\text{Pb}_{\text{ex}}$ , may obscure any distinct large scale geographic differences in seafloor accumulation within the central Barents Sea. In the present study, we

report an average  $^{210}\text{Pb}_{\text{ex}}$  sedimentation rate of  $558 \pm 154 \text{ g m}^{-2}\text{y}^{-1}$  and an average sedimentation velocity of  $1.1 \pm 0.4 \text{ mm y}^{-1}$  ( $n = 7$ ).  $^{137}\text{Cs}$  derived sedimentation velocities average  $1.0 \pm 0.4 \text{ mmy}^{-1}$  ( $n = 7$ ). However it is important to note that two out of the nine sediment cores exhibited uniform  $^{210}\text{Pb}_{\text{ex}}$  and  $^{137}\text{Cs}$  profiles, suggestive of complete mixing with no sediment accumulation (Figs. 3 and 5). Smith et al. (1995) evaluated sedimentation and mixing rates at two locations in the Barents Sea,  $< 50$  km offshore from the underwater nuclear test site at Chernaya Bay in the south-west corner of Novaya Zemlya. Using a similar model to that described here, they obtained comparable sediment velocities of 1.2 and  $2.7 \text{ mmy}^{-1}$  below the mixed layer and mixing coefficients of 0.5 and  $2.3 \text{ cm}^2\text{y}^{-1}$ .

### 3.3. Radionuclide inventories

Average  $^{210}\text{Pb}_{\text{ex}}$  inventories for POW, MIC and PIC are  $1.0 \pm 0.2$ ,  $1.4 \pm 0.3$  and  $0.5 \pm 0.2 \text{ Bq cm}^{-2}$ , respectively (Fig. 7) with statistically significant differences among the regions ( $p = 0.012$ ). The  $^{210}\text{Pb}_{\text{ex}}$  inventory in sediment cores from the PIC is significantly lower than in the MIC (post hoc Tukey;  $p = 0.01$ ). This may be due to less atmospherically derived  $^{210}\text{Pb}$  (Preiss et al., 1996; Preiss and Genthon, 1997) as the PIC has the highest frequency of ice cover throughout the year. In general the area also receives minimal terrigenous input due to its distance from the coast and the flow paths of the major rivers (Fransson et al. 2001).

We estimate the  $^{210}\text{Pb}_{\text{ex}}$  inventory for the region as follows:

$$^{210}\text{Pb}_{\text{ex}} \text{ inventory} = [(A_{226\text{Ra}} - A_{210\text{Pb}}) \times \lambda_{\text{Pb}} \times z + A_{210\text{Pbatm}}] \times \tau_{\text{Pb}}$$

where  $A_{226\text{Ra}}$  is the  $^{226}\text{Ra}$  water column activity,  $A_{210\text{Pb}}$  is the  $^{210}\text{Pb}$  water column activity,  $A_{210\text{Pbatm}}$  is the activity of atmospheric  $^{210}\text{Pb}$  input,  $\lambda_{\text{Pb}}$  is the  $^{210}\text{Pb}$  decay constant,  $\tau_{\text{Pb}}$  is the mean life of  $^{210}\text{Pb}$  and  $z$  is the depth of the water column. Water column  $^{226}\text{Ra}$  data derived from the Transient Tracer in Ocean (TTO) – North Atlantic Series database from station location  $78.53^\circ\text{N}\text{--}9.47^\circ\text{E}$  (Key et al., 1992). This station is located just to the west of the study area. The dissolved  $^{210}\text{Pb}$  concentration is assumed to be 0, implying that all  $^{210}\text{Pb}$  is scavenged from the water column to sediments; thus our determined inventories are upper limit estimates. The atmospheric  $^{210}\text{Pb}$  flux reported from Svalbard, Norway (Fig. 1), located near the northwestern corner of the study area is  $0.44 \text{ dpm cm}^{-2}\text{y}^{-1}$  (Preiss and Genthon, 1997). Using this data, the average expected  $^{210}\text{Pb}_{\text{ex}}$  inventory for the study

area is calculated to be  $0.27 \pm 0.01 \text{ Bq cm}^{-2}$ . The  $^{210}\text{Pb}$  inventories calculated from the sediment cores are much higher than the expected inventories for all the three regions by a factor of 3.8, 5.2 and 1.9 for POW, MIC and PIC respectively. Others (e.g. Lepore et al., 2009) have also reported higher than expected  $^{210}\text{Pb}$  inventories for sediments from the Arctic region. The MIC has approximately a four-fold higher  $^{210}\text{Pb}$  inventory suggesting that MIC is an important sink for  $^{210}\text{Pb}$ . This is probably due to the combination of both sediment focusing and input of excess  $^{210}\text{Pb}$  by ice-rafted sediments (IRS),

which have been reported to be highly enriched in excess  $^{210}\text{Pb}$  (Baskaran et al., 2003; Masqué et al., 2007).

In contrast, a statistical comparison of  $^{234}\text{Th}_{\text{ex}}$  sediment inventories by region for all stations yielded a significant regional relationship (1 way ANOVA,  $p=0.026$ ). Mean  $^{234}\text{Th}_{\text{ex}}$  sediment inventories were significantly higher in the MIC region ( $191 \pm 40 \text{ Bq m}^{-2}$ ) when compared to either the PIC ( $82 \pm 33 \text{ Bq m}^{-2}$ ) or POW ( $90 \pm 44 \text{ Bq m}^{-2}$ ) (post hoc Tukey;  $p<0.05$ ), while both PIC and POW means were similar ( $p=0.97$ ). A higher  $^{234}\text{Th}$  inventory for

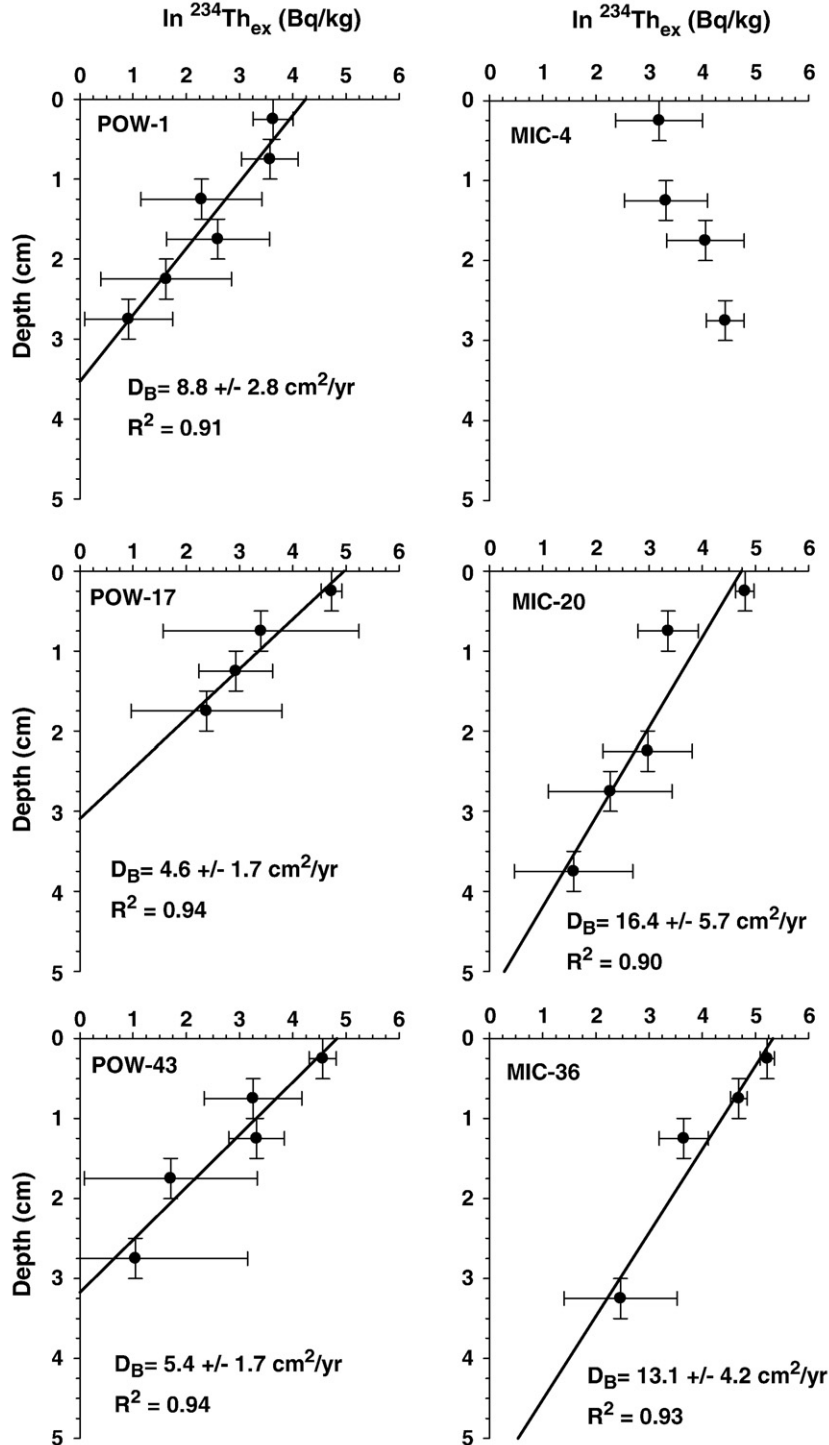


Fig. 4. Profiles of  $^{234}\text{Th}_{\text{ex}}$  versus sediment depth ( $z$ ). The linear regression best fit to the  $^{234}\text{Th}_{\text{ex}}$  versus depth  $z$  is shown (solid line). Sediment mixing rates ( $D_B$ ) were derived in accordance with Eq. (7).

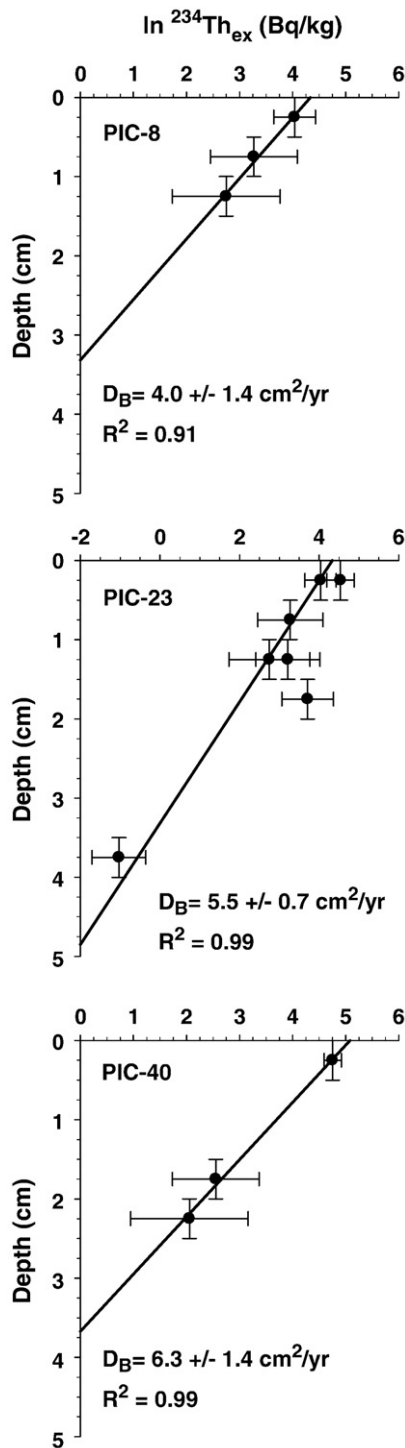


Fig. 4 (continued).

the MIC indicates that this zone has higher particle scavenging and vertical flux (at least during summer/spring 2003), probably due to the higher primary productivity in this region.

$^{137}\text{Cs}$  sediment inventories vary from 94 to 406  $\text{Bq m}^{-2}$  (Fig. 6), averaging  $221 \pm 42 \text{ Bq m}^{-2}$  in the POW,  $325 \pm 93 \text{ Bq m}^{-2}$  in the MIC, and  $239 \pm 128 \text{ Bq m}^{-2}$  in the PIC. There are no statistically significant differences in  $^{137}\text{Cs}$  inventories among regions implying that there is no geographic trend for this tracer in the central Barents Sea. We attribute this to a combination of mixed sediment supplies and multiple contamination sources of  $^{137}\text{Cs}$ . The dominant

source of  $^{137}\text{Cs}$  for Barents Sea is from the direct discharge of radioactive waste into the waters of the Irish and North Seas from fuel reprocessing facilities at Sellafield (west) and the weapons-testing facility at Novaya Zemlya (east) followed by Chernobyl and riverine inputs (south and east). Ice-rafted sediments, enriched in  $^{137}\text{Cs}$ , may also supply  $^{137}\text{Cs}$  to the seafloor (Masqué et al., 2007). These different sources of  $^{137}\text{Cs}$  bring different activities and amounts of  $^{137}\text{Cs}$  to the central Barents Sea, resulting in complex sediment inventory records. The impact of physical and biological processes on the flux of  $^{137}\text{Cs}$  into the sediments is hence difficult to interpret, particularly in context with the other natural radioisotope inventories e.g.  $^{210}\text{Pb}$  or  $^{234}\text{Th}$ .

### 3.4. Nutrient patterns

Sediment layers from six out of the nine cores were analyzed for  $C_{\text{tot}}$ ,  $C_{\text{org}}$ , and  $N_{\text{tot}}$  (Table 1). Cores were chosen to provide the least disturbed, but longest sediment record. Comparing average nutrient content within the surface mixed layer ( $z^*$ ), both  $C_{\text{org}}$  and  $N_{\text{tot}}$  are relatively high within the MIC and PIC compared to POW. The sediments for MIC have a higher average  $C_{\text{org}}$  content of  $2.0\% \pm 0.2\%$  compared to PIC ( $1.6\% \pm 0.1\%$ ) and POW ( $1.4\% \pm 0.1\%$ ).

The fluxes of  $C_{\text{org}}$  and  $N_{\text{tot}}$  at the seafloor surface are estimated by multiplying sedimentation rates ( $\text{g cm}^{-2} \text{y}^{-1}$ ) by the average elemental content of the surface mixed layer at each station (Fig. 8). Although nutrient levels in the MIC are relatively enriched compared to the other two regions, the relatively small differences in  $^{210}\text{Pb}_{\text{ex}}$  derived sedimentation rates among stations obfuscate any clear signal of enhanced nutrient deposition within the MIC region over the detection time-scale of  $^{210}\text{Pb}_{\text{ex}}$ . Cochran et al. (2009) estimated the annual integrated water column productivity for each of the stations using the SINMOD hydrodynamical–chemical–biological ecosystem model for the Barents Sea (Wassmann et al., 2006). Comparing water column primary productivity with the flux of  $C_{\text{org}}$  at the seafloor surface gives a burial efficiency of  $5.3 \pm 2.5\%$ ,  $17.5 \pm 8.8\%$  and  $18.4 \pm 1.6\%$  for POW, MIC and PIC respectively. This indicates that MIC and PIC may be more efficient in organic carbon burial, receiving a greater percentage of pelagic production compared to POW. A similar range in organic carbon burial rates has been reported for the northwestern Barents Sea where about 6% of the annual integrated primary productivity or 15% of the vertical flux is transferred to the Barents Sea sediment–water interface (Zaborska et al., 2008).

Few measurements of  $P_{\text{org}}$  are available for Arctic shelf seas. Here we report values for two stations, POW-1 and MIC-4. Average  $P_{\text{org}}$  contents in the surface mixed layer at these stations are  $0.015 \pm 0.001\%$  and  $0.018 \pm 0.001\%$ , respectively. The corresponding fluxes derived using the same approach as described above for  $C_{\text{org}}$  and  $N_{\text{tot}}$  are  $0.054 \pm 0.006 \text{ g P m}^{-2} \text{y}^{-1}$  at POW-1 and  $0.098 \pm 0.010 \text{ g P m}^{-2} \text{y}^{-1}$  at MIC-4. These results further support the above conclusion that the MIC is more efficient in organic matter burial.

## 4. Implications and conclusions

Pelagic–benthic coupling is a feature of the Barents Sea ecosystem associated with the seasonal onset of the spring bloom in this Arctic marginal sea. Surface sediments within the MIC exhibit higher bioturbation rate coefficients, higher  $^{234}\text{Th}_{\text{ex}}$  sediment inventories, and higher  $C_{\text{org}}$ ,  $N_{\text{tot}}$  concentrations in comparison with the other regions, especially with respect to POW. Given that POW sediments receive a relatively small proportion of the pelagic productivity compared to MIC and PIC, a widening of POW further north could result in a lower proportion of pelagic production reaching the sediments to sustain the benthic community. This corresponds well with previous studies of enhanced primary production and export flux at the ice edge during the spring bloom within the Barents Sea (Wassmann and Slagstad, 1993; Wassmann et al., 1999; Reigstad et al.,

2002). There is also a significant correlation between surface sediment chlorophyll-*a* and integrated water column chlorophyll-*a* for the Western Barents Sea, suggesting that local water column and ice-algae productivity is the major source of fresh organic carbon for the benthos (Morata and Renaud, 2008). The data here, although limited, provide further evidence in support of a tight coupling between pelagic and benthic ecosystems during this short, intense melting period at the ice edge. In particular, the correlation between benthic individuals and  $^{234}\text{Th}_{\text{ex}}$  bioturbation rates provide strong evidence that sediment mixing in the central Barents Sea is linked to biological activity and that sediments below the MIC exhibit enhanced

mixing compared to the adjacent POC and PIC areas.  $^{234}\text{Th}_{\text{ex}}$  bioturbation rate coefficients (ranging from 4.0 to 16  $\text{cm}^2\text{y}^{-1}$ ) are an order of magnitude higher than those derived from  $^{210}\text{Pb}_{\text{ex}}$ .  $^{210}\text{Pb}_{\text{ex}}$  sedimentation rates and velocities, assuming negligible  $D_B$  below a surface mixed depth, are relatively uniform throughout the central Barents Sea, averaging  $558 \pm 154 \text{ g m}^{-2}\text{y}^{-1}$  and  $1.1 \pm 0.4 \text{ mm y}^{-1}$ .  $^{137}\text{Cs}$  sedimentation velocities confirm the  $^{210}\text{Pb}$  derived estimates, providing confidence in results.

Model estimates currently suggest that the polar ice pack will be reduced by 20% in winter and 80% in summer by the end of this century (Johannessen et al., 2004). This northward retreat of the MIC

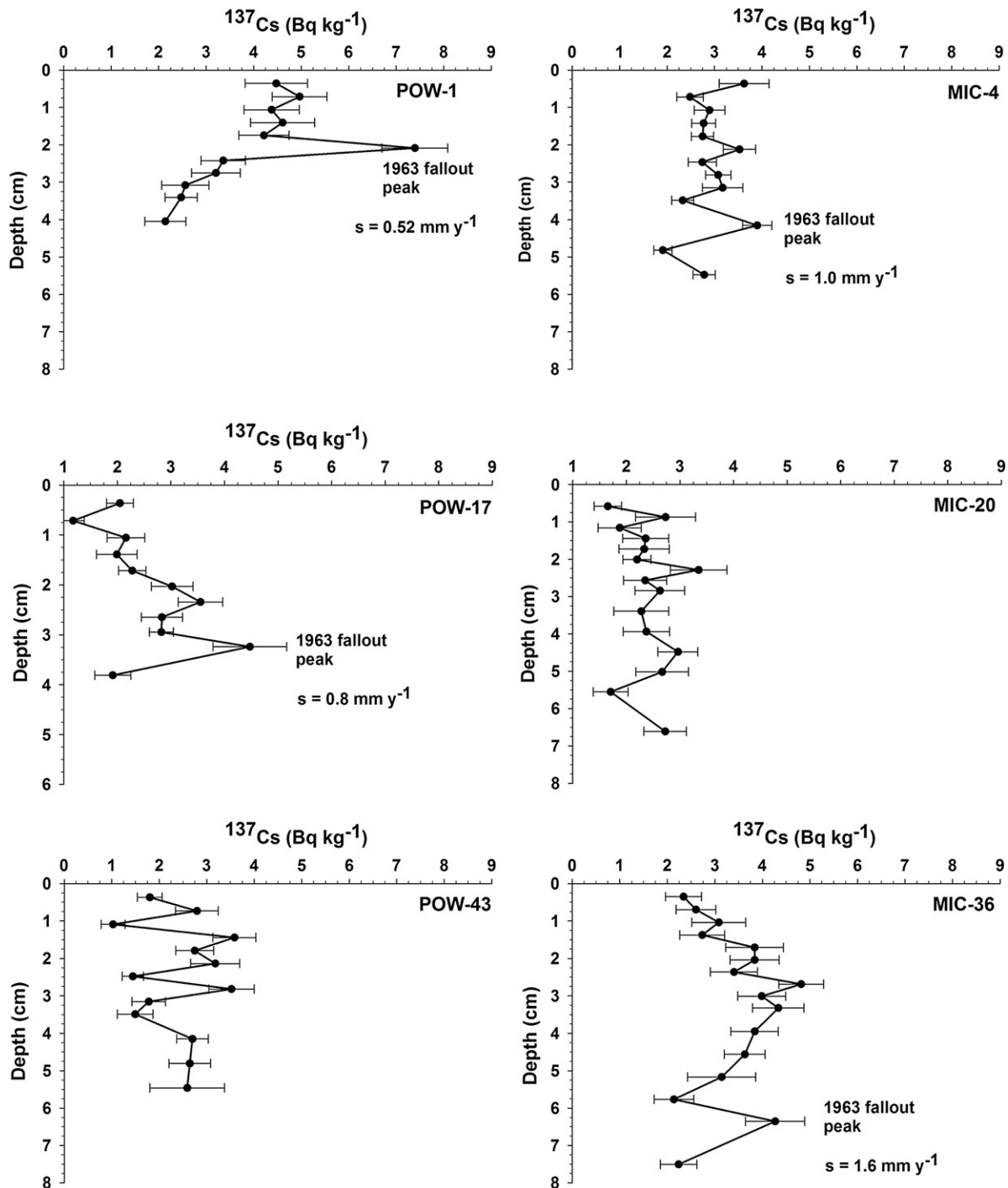


Fig. 5. Profiles of  $^{137}\text{Cs}$  versus sediment depth (*z*).  $^{137}\text{Cs}$  sedimentation velocities ( $\text{mm y}^{-1}$ ) were calculated assuming that the depth of the maximum in  $^{137}\text{Cs}$  activity is attributed to the 1963 peak in atmospheric fallout from nuclear weapon testing.

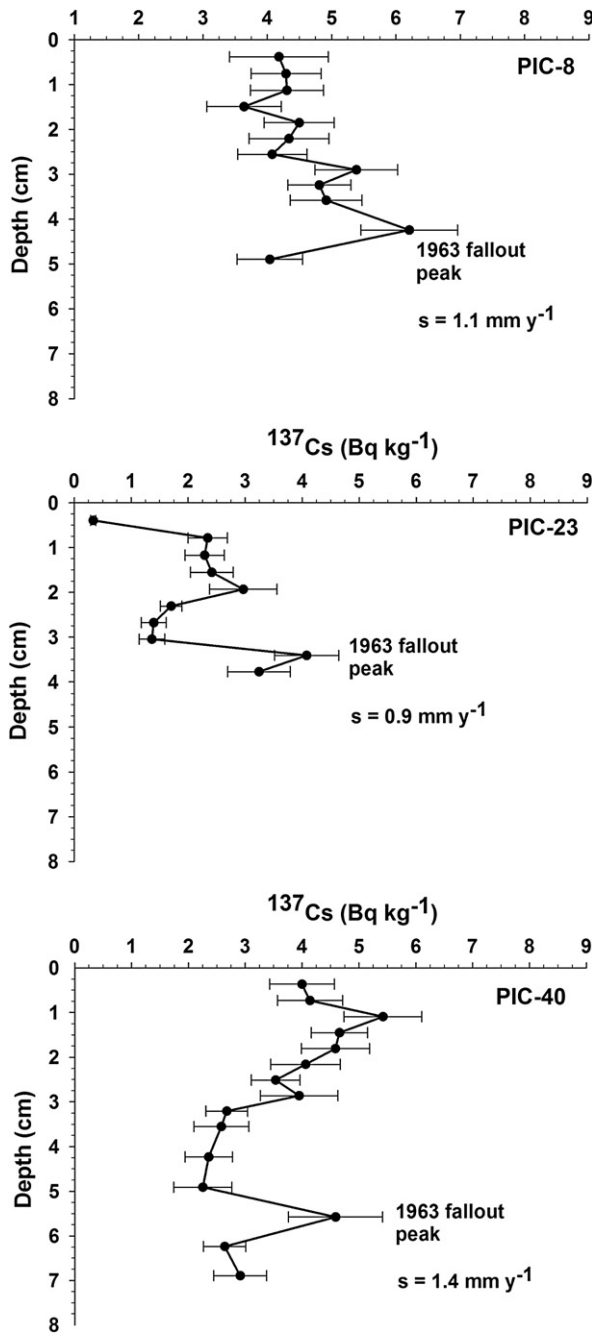


Fig. 5 (continued).

will likely result in a larger SIZ and a more extensive, stratified area that stretches further north. A change in the position and extent of the SIZ will not only greatly affect the magnitude and locus of primary production, but also the amount and composition of particles that reach the seafloor. A northward retreat of the MIZ and PIC would also mean that these areas will be located over deeper parts of the Barents Sea than present and may result in more water column remineralisation of organic carbon before it reaches the seafloor. Such alterations will undoubtedly induce changes in both the quality and quantity of food available to support benthic ecosystems (Carroll and Carroll, 2003; McMahon et al., 2006; Wassmann et al., 2006). The coupling between food supply and benthos needs to be further studied in order to confirm these results and to derive realistic scenarios of future climate change impacts for different

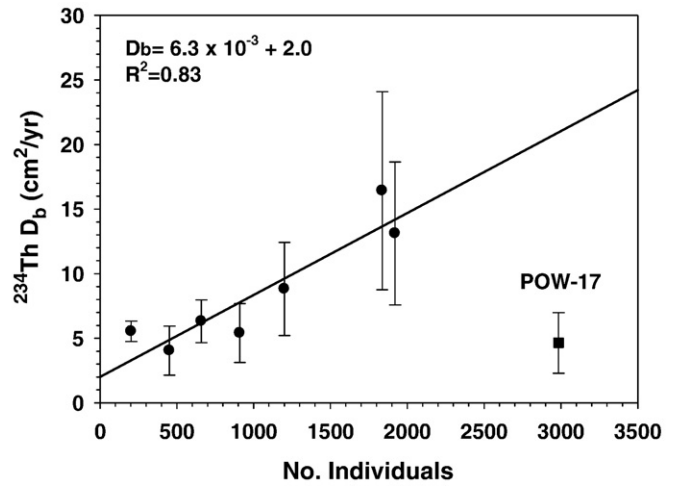


Fig. 6.  $^{234}\text{Th}_{\text{ex}}$  bioturbation rates ( $D_b$ ) versus number of benthic individuals per  $0.5 \text{ m}^2$ . The solid line represents the linear regression best fit relationship excluding station POW-17.

arctic marginal seas.  $^{234}\text{Th}_{\text{ex}}$  also appears to be a highly valuable tracer of short-term benthic responses to pelagic supplies of primary production in arctic marginal seas.

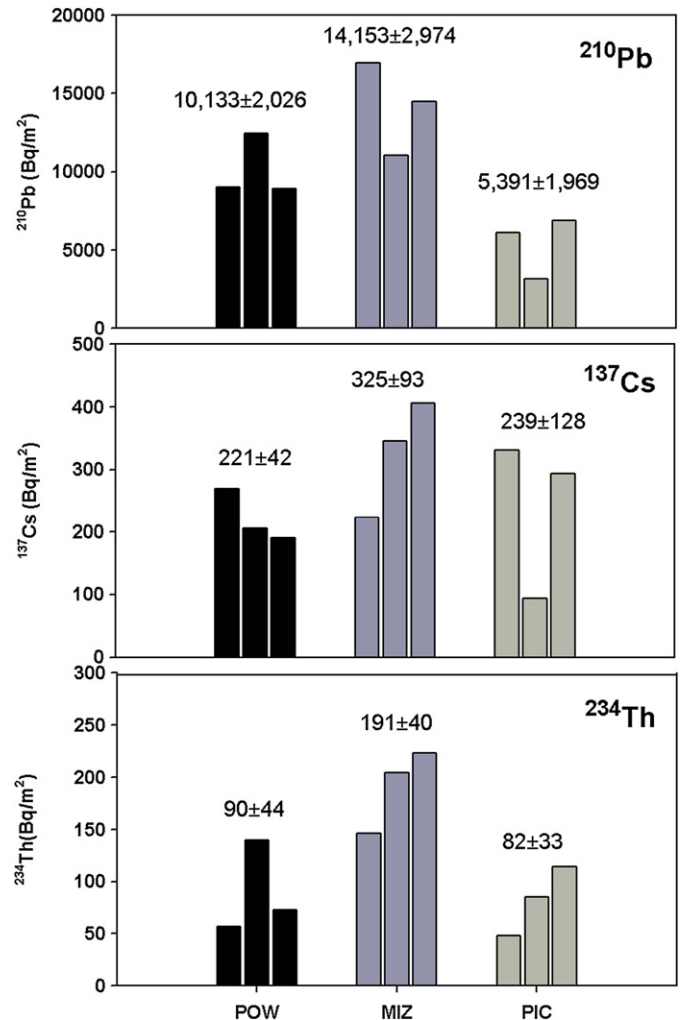


Fig. 7.  $^{210}\text{Pb}_{\text{ex}}$ ,  $^{137}\text{Cs}$  and  $^{234}\text{Th}_{\text{ex}}$  inventories for stations grouped by region: POW, MIZ, and PIC.

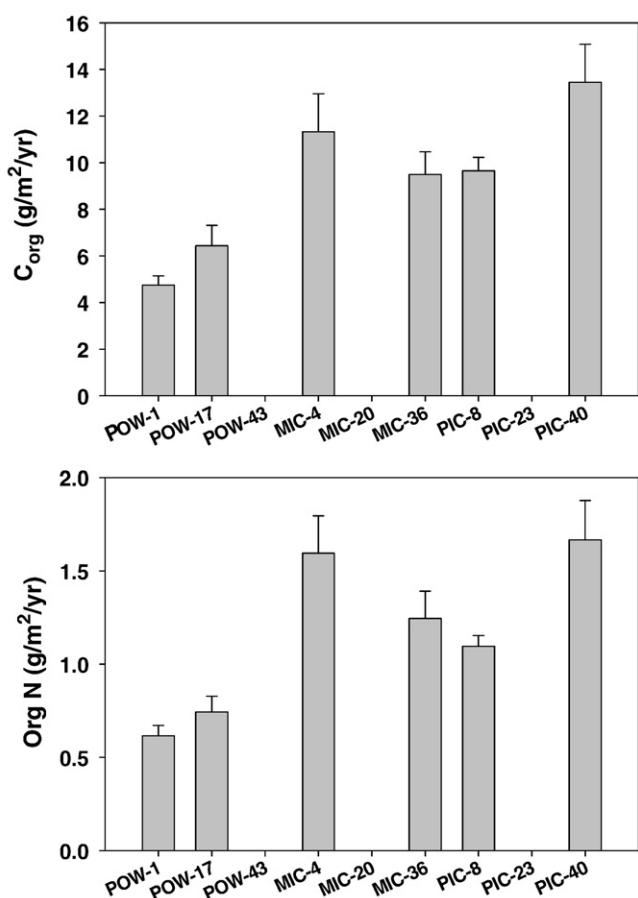


Fig. 8.  $C_{org}$  and  $N_{tot}$  sedimentation rates. Cores from stations POW-43, MIZ-20, and PIC-23 were not analyzed for  $C_{org}$  and  $N_{tot}$ . Only cores from stations POW-1 ( $0.054 \pm 0.006 \text{ g P m}^{-2} \text{ y}^{-1}$ ) and MIC-4 ( $0.098 \pm 0.010 \text{ g P m}^{-2} \text{ y}^{-1}$ ) were analyzed for  $P_{org}$ .

## Acknowledgements

This study was financed by the Norwegian Research Council East European Programme (NFR Grant# 152798/V10). Thanks to the crew of R/V *Ivan Petrov* and to Sabine Cochrane, Chris Emblow and Harvard Dahle for assistance in collection and processing of cores. CHN analyses were performed with the assistance of Eric Tappa and Megan Luc and particulate phosphorus analyses were determined with help from Renee Styles. We would like to acknowledge Dr. Willard Moore and Dr. Ian Lerche for their insightful discussions and helpful comments. We also wish to thank the anonymous reviewers for their many valuable suggestions which have improved this contribution.

## References

- Aller, R.C., Cochran, J.K., 1976. Th-234/U-238 disequilibrium in nearshore sediments: particle reworking and diagenetic time scales. *Earth Planet. Sci.* 29, 37–50.
- Aller, R.C., Demaster, D.J., 1984. Estimates of particle flux and reworking at the deep-sea floor using  $^{234}\text{Th}/^{238}\text{U}$  disequilibrium. *Earth Planet. Sci.* 47, 161–175.
- Alperin, M.J., Martens, C.S., Albert, D.B., Suayah, I.B., Benninger, L.K., Blair, N.E., Jahnke, R.A., 1999. Benthic fluxes and porewater concentration profiles of dissolved organic carbon in sediments from the North Carolina continental slope. *Geochim. Cosmochim. Acta* 63, 427–448.
- Anderson, R., Bopp, R., Buesseler, K.O., Biscaye, P., 1988. Mixing of particles and organic constituents in sediments from continental shelf off Cape Cod: SEEP-I results. *Cont. Shelf Res.* 8 (5–7), 925–946.
- Appleby, P.G., 2001. In: Last, W., Smol, J. (Eds.), *Chronostratigraphic Techniques in Recent Sediments: Tracking Environmental Change Using Lake Sediments*, vol. 1. Kluwer Academic Publishers, Dordrecht.
- Appleby, P.G., Oldfield, F., 1992. The calculation of lead-210 dates assuming a constant rate of supply of unsupported  $^{210}\text{Pb}$  to the sediment. *Catena* 5, 1–8.
- Aspila, K.I., Agemian, H., Chau, A.S., 1976. A semi-automated method for the determination of inorganic, organic and total phosphate in sediments. *Analyst* 101, 187–197.
- Athy, L.F., 1930. Density, porosity, and compaction of sedimentary rocks. *AAPG Bull.* 14, 1–22.
- Baskaran, M., Swarzenski, P.W., Porcelli, D., 2003. Role of colloidal material in the removal of  $^{234}\text{Th}$  in the Canada basin of the Arctic Ocean. *Deep Sea Research Part I: Oceanographic Research Papers* 50, 1353–1373.
- Bellec, V., Wilson, M., Bøe, R., Rise, L., Thorsnes, T., Mortensen, L.B., Mortensen, P.B., 2008. Bottom currents interpreted from iceberg ploughmarks revealed by multi-beam data at Tromsøflaket, Barents Sea. *Mar. Geol.* 249, 257–270.
- Cambay, R., Cawse, P., Garland, J., Gibson, J., Johnson, P., Lewis, G., Newton, D., Salmon, L., Wade, B., 1987. Observations on radioactivity from the Chernobyl accident. *Nucl. Energy* 26, 77–101.
- Carmack, E., Wassman, P., 2006. Food webs and physical-biological coupling on pan-arctic shelves: comprehensive perspectives, unifying concepts and future research. *Prog. Oceanogr.* 71, 446–477.
- Carroll, M.L., Carroll, J., 2003. The Arctic Seas. In: Black, K.D., Shimmield, G.B. (Eds.), *Biogeochemistry of Marine Systems*. Blackwell Publishing, pp. 127–156.
- Carroll, J., Lerche, I., 2003. *Sedimentary Processes: Quantification Using Radionuclides*. Elsevier, 272 pp.
- Carroll, M.L., Denisenko, S., Renaud, P., Ambrose, W., 2008a. Benthic infauna of the marginally ice-covered western Barents Sea: latitudinal patterns and relationships to physical forcing. *Deep-Sea Res. II* 55, 2340–2351.
- Carroll, J., Zaborska, A., Papucci, C., Pempkowiak, J., 2008b. Sediment burial processes and the preservation of organic matter on the seafloor of the western Barents Sea. *Deep-Sea Res. II* 55, 2361–2371.
- Carter, M., Moghissii, A., 1977. Three decades of nuclear testing. *Health Phys. Press.* 33, 55–71.
- Cochran, J.K., 1992. The Oceanic Chemistry of the Uranium and Thorium-series Nuclides. In: Ivanovich, M., Harmon, R.S. (Eds.), *Uranium-series Disequilibrium: Applications to Earth, Marine, and Environmental Sciences*. Oxford University Press, New York, pp. 334–395.
- Cochrane, S.K.J., Denisenko, S.G., Renaud, P.E., Emblow, C.S., Ambrose Jr., W.G., Ellingsen, I.H., Skarøhamar, J., 2009. Benthic macrofauna and productivity regimes in the Barents Sea – ecological implications in a changing Arctic. *J. Sea Res.* 61, 222–233.
- Comiso, J.C., Parkinson, C.L., Gersten, R., Stock, L., 2008. Accelerated decline in the Arctic sea ice cover. *Geophys. Res. Lett.* 35, L01703.
- Crusius, J., Bothner, M., Sommerfield, C.K., 2004. Bioturbation depths, rates and processes in Massachusetts Bay sediments inferred from modeling of  $^{210}\text{Pb}$  and  $^{239+240}\text{Pu}$  profiles. *Est. Coast and Shelf Sci.* 61 (4), 643–655.
- DeMaster, D.J., McKee, B.A., Nittroer, C.A., Brewster, D.C., Biscaye, P.E., 1985. Rates of sediment reworking at the HEBBLE site based on measurements of Th-234, Cs-137, and Pb-210. *Mar. Geol.* 66, 133–148.
- Deser, C., Teng, H., 2008. Evolution of Arctic sea ice concentration trends and the role of atmospheric forcing, 1979–2007. *Geophys. Res. Lett.* 35, L02504. doi:10.1029/2007GL032023.
- Dunton, K., Goodall, J.L., Schonberg, S.V., Grebmeier, J.M., Maidment, D.R., 2005. Multi-decadal synthesis of benthic–pelagic coupling in the western arctic: role of cross-shelf advective processes. *Deep-Sea Res. II* 52, 3462–3477.
- Fransson, A., Chierici, M., Anderson, L.G., Bussmann, I., Kattner, G., Peter Jones, E., Swift, J.H., 2001. The importance of shelf processes for the modification of chemical constituents in the water of the Eurasian Arctic Ocean: implication for carbon flux. *Cont. Shelf Res.* 21, 225–242.
- Gerino, M., Aller, R.C., Lee, C., Cochran, J.K., Aller, J.Y., Green, M.A., Hirschberg, D., 1998. Comparison of different tracers and methods used to quantify bioturbation during a spring bloom:  $^{234}\text{thorium}$ , luminophores and chlorophyll a. *Estuar. Coast. Shelf Sci.* 46, 531–547.
- Grebmeier, J.M., Overland, J.E., Moore, S.E., Farley, E.V., Carmack, E.C., Cooper, L.W., Frey, K.E., Helle, J.H., McLaughlin, F.A., Mcnutt, S.L., 2006. A major ecosystem shift in the northern Bering Sea. *Science* 311, 1461–1464.
- Hedges, J.I., Stern, J.H., 1984. Carbon and nitrogen determinations of carbonate-containing solids. *Limnol. Oceanogr.* 29 (3), 657–663.
- Huh, C., Pisiias, N.G., Kelley, J.M., Maiti, T.C., Grantz, A., 1997. Natural radionuclides and plutonium in sediments from the western Arctic Ocean: sedimentation rates and pathways of radionuclides. *Deep-Sea Res. II* 44 (8), 1725–1743.
- Ivanova, E.V., Murdmaa, I.O., Duplessy, J.C., Paterne, M., 2002. Late Weichselian to Holocene paleoenvironments in the Barents Sea. *Glob. Planet. Change* 34, 209–218.
- Johannessen, O.M., Bengtsson, L., Miles, M.W., Kuzmina, S.I., Semenov, V.A., Alekseev, G.V., Nagurnyi, A.P., Zakharov, V.F., Bobylev, L.P., Petterson, L.H., Hasselmann, K., Cattle, H.P., 2004. Arctic climate change: observed and modelled temperature and sea-ice variability. *Tellus* 56A, 328–341.
- Keup-Thiel, E., Goettel, H., Jacob, D., 2006. Regional climate simulations for the Barents Sea region. *Boreal Environ. Res.* 11, 329–339.
- Key, R.M., Moore, W.S., Sarmiento, J.L., 1992. *Transient Tracer in the Ocean – North Atlantic Series, Final Data Report for  $^{228}\text{Ra}$  and  $^{226}\text{Ra}$* . OTL Technical Report No. 92-2, Princeton University, Princeton, NJ 08544.
- Krishnaswami, S., Benninger, L.K., Aller, R.C., Von Damm, K.L., 1980. Atmospherically derived radionuclides as tracers of sediment mixing and accumulation in near shore marine and lake sediments: evidence from 7Be,  $^{210}\text{Pb}$  and  $^{239, 240}\text{Pu}$ . *Earth Planet. Sci. Lett.* 47, 307–318.
- Lepore, K., Moran, S.B., Smith, J.N., 2009.  $^{210}\text{Pb}$  as a tracer of shelf-basin transport and sediment focusing in the Chukchi Sea. *Deep-Sea Res. II* 56, 1305–1315.
- Lima, A.L., Hubeny, J.B., Reddy, C.M., King, J.W., Hughen, K.A., Eglington, T.I., 2005. High-resolution historical records from Pettaquamscutt river basin sediments:  $^{210}\text{Pb}$  and varve chronology validate record of  $^{137}\text{Cs}$  released by the Chernobyl accident. *Geochim. Cosmochim. Acta* 69 (7), 1803–1812.

- Masqué, P., Cochran, J.K., Hirschberg, D.J., Dethleff, D., Hebbeln, D., Winkler, A., Pfriman, S., 2007. Radionuclides in Arctic sea ice: tracers of sources, fates and ice transit time scales. *Deep-Sea Res.* 54 (8), 1289–1310.
- Matsumoto, E., 1975.  $^{210}\text{Pb}$  geochronology of sediments from Lake Shinji. *Geochem. J.* 9, 167–172.
- McMahon, K.W., Johnson, B.J., Sun, M.Y., Lopez, G.R., Clough, L.M., Carroll, M.L., 2006. Benthic community response to ice algae and phytoplankton in Ny Ålesund, Svalbard. *Mar. Ecol. Prog. Ser.* 310, 1–14.
- Meysman, F.J.R., Boudreau, B.P., Middelburg, J.J., 2005. Modeling reactive transport in sediments subject to bioturbation and compaction. *Geochem. Cosmochim. Acta* 69, 3601–3617.
- Miller, R.J., Smith, C.R., DeMaster, D.J., Fornes, W.I., 2000. Feeding selectively and rapid particle processing by deep-sea megafaunal deposit feeders: a  $^{234}\text{Th}$  approach. *J. Mar. Res.* 58, 653–673.
- Morata, N., Renaud, P.E., 2008. Sedimentary pigments in the western Barents Sea: a reflection of pelagic–benthic coupling? *Deep-Sea Res. II* 55, 2381–2389.
- Phillips, G.W., Marlow, K.W., 1976. Automatic analysis of gamma-ray spectra from germanium detectors. *Nucl. Instrum. Methods* 137, 525–536.
- Piepenburg, T.H., Blackburn, vonDorrien, C.F., Gutt, J., Hall, P.O.J., Hulth, S., Kendall, M.A., Opalinski, K.W., Racher, E., Schmid, M.K., 1995. Partitioning of benthic community respiration in the Arctic (Northwestern Barents Sea). *Mar. Ecol. Prog. Ser.* 118, 119–213.
- Polyakov, I.V., Beszczynska, A., Carmack, E.C., Dmitrenko, I.A., Fahrback, E., Frolov, I.E., Gerdes, R., Hansen, E., Holfort, J., Ivanov, V.V., Johnson, M.A., Karcher, M., Kauker, F., Morison, J., Orvik, K.A., Schauer, U., Slimmons, H.L., Skagseth, Ø., Sokolov, V.T., Steele, M., Timokhov, L.A., Walsh, D., Walsh, J.E., 2005. One more step towards a warmer Arctic. *Geophys. Res. Lett.* 32, L17605. doi:10.1029/2005GL023740.
- Pope, R.H., DeMaster, D.J., Smith, C.R., Seltnmann, H., 1996. Rapid bioturbation in equatorial Pacific sediments: evidence from excess  $^{234}\text{Th}$  measurements. *Deep-Sea Res. II* 43, 1339–1364.
- Preiss, N., Genthon, C., 1997. Use of a new database of lead-210 for global aerosol model validation. *J. Geophys. Res.* 102 (D21), 25347–25357.
- Soetaert, K., Herman, P.M.J., Middelburg, J.J., Hei, C., deStigter, H.S., van Weering, T.C.E., Epping, E., Helder, W., 1996. Modeling  $^{210}\text{Pb}$ -derived mixing activity in ocean margin sediments: diffusive versus non-local mixing. *J. Mar. Res.* 54, 1207–1227.
- Preiss, N., Melieres, M., Pourchet, M., 1996. A compilation of data on lead-210 concentration in surface air and fluxes at the air–surface and water–sediment interfaces. *J. Geophys. Res.* 101 (D22), 28847–28862.
- Reigstad, M., Wassmann, P., Wexels Riser, C., Oygarden, S., Rey, F., 2002. Variation in hydrography, nutrients and chlorophyll a in the marginal ice zone and the central Barents Sea. *J. Mar. Syst.* 38, 9–29.
- Renaud, P., Morata, N., Carroll, M.L., Denisenko, S.G., Reigstad, M., 2008. Pelagic–benthic coupling in the western Barents Sea: processes and time-scales. *Deep-Sea Res.* 55, 2372–2380.
- Ritchie, J.C., McHenry, J.R., 1990. Application of radioactive fallout cesium-137 for measuring soil erosion and sediment accumulation rates and patterns: a review. *J. Environ. Qual.* 19, 215–233.
- Robbins, A., 1978. Geochemical and Geophysical Applications of Radioactive Lead Isotopes. In: Nriagu, J.P. (Ed.), *Biogeochemistry of Lead*. North Holland, Amsterdam, pp. 285–393.
- Schauer, U., Loeng, H., Rudels, B., Ozhigin, V.K., Dieck, W., 2002. Atlantic water flow through the Barents and Kara Seas. *Deep-Sea Res.* 49, 2281–2298.
- Serreze, M.C., Maslanik, J.A., Scambos, T.A., Fetterer, F., Stroeve, J., Knowles, K., Fowler, C., Drobot, S., Barry, R.G., Haran, T.M., 2003. A record minimum Arctic sea ice extent and area in 2002. *Geophys. Res. Lett.* 30 (3), 11101–11104.
- Smith, J.N., Boudreau, B.P., Noshkin, V., 1986/87. Plutonium and  $^{210}\text{Pb}$  distributions in northeast Atlantic sediments: subsurface anomalies caused by non-local mixing. *Earth Planet. Sci. Lett.* 81, 15–28.
- Smith, J.N., Ellis, K.M., Naes, K., Dahle, S., Matishov, D., 1995. Sedimentation and mixing rates of radionuclides in Barents Sea sediments off Novaya Zemlya. *Deep-Sea Res. II* 42 (6), 1471–1493.
- Smoak, J.M., Moore, W.S., Thunell, R.C., 2000. Influence of boundary scavenging and sediment focusing on  $^{234}\text{Th}$ ,  $^{228}\text{Th}$  and  $^{210}\text{Pb}$  fluxes in the Santa Barbara Basin. *Estuar. Coast. Shelf Sci.* 51 (3), 373–384.
- Smith, J.N., Moran, S.B., Macdonald, R.W., 2003. Shelf-basin interactions in the Arctic Ocean based on  $^{210}\text{Pb}$  and Ra isotope tracer distributions. *Deep-Sea Res.* 50, 397–416.
- Wassmann, P., Slagstad, D., 1993. Marginal and annual dynamics of particulate carbon flux in the Barents Sea. *Polar Biol.* 13, 363–372.
- Wassmann, P., Ratkova, T.N., Andreassen, I.J., Vernet, M., Pedersen, G., Rey, F., 1999. Spring bloom development in the Marginal Ice Zone and the central Barents Sea. *Mar. Ecol. Prog. Ser.* 170, 321–346.
- Stein, R., Macdonald, R.W., 2004. Organic Carbon Budget: Arctic vs. Global Ocean. In: Stein, R., Macdonald, R.W. (Eds.), *The Organic Carbon Cycle in the Arctic Ocean*. Berlin Heidelberg, Springer-Verlag, pp. 315–322.
- Stroeve, J., Holland, M.M., Meier, W., Scambos, T., Serreze, M., 2007. Arctic sea ice decline: faster than forecast. *Geophys. Res. Lett.* 34, L09501.
- Tamelander, T., Renaud, P.E., Hop, H., Carroll, M.L., Ambrose, W.G., Hobson, K.A., 2006. Trophic relationships and pelagic–benthic coupling during summer in the Barents Sea Marginal Ice Zone, revealed by stable carbon and nitrogen isotope measurements. *Mar. Ecol. Prog. Ser.* 310, 33–46.
- Turekian, K.K., Nozaki, Y., Benninger, L.K., 1977. Geochemistry of atmospheric radon and radon products. *Annu. Rev. Earth Planet. Sci.* 5, 227–255.
- Vinje, T., 2001. Anomalies and trends of sea-ice extent and atmospheric circulation in the Nordic Seas during the period 1864–1998. *J. Clim.* 14, 255–267.
- Wassmann, P., 1991. Dynamics of primary production and sedimentation in shallow fjords and pols of western Norway. *Ocean. Mar. Bio. Ann. Rev.* 29, 87–154.
- Wassmann, P., Reigstad, M., Haug, T., Rudels, B., Carroll, M.L., Hop, H., Gabrielsen, G.W., Falk-Petersen, S., Denisenko, S.G., Arashkevich, E., Slagstad, D., Pavlova, O., 2006. Food web and carbon flux in the Barents Sea. *Progr. Ocean.* 71, 232–287.
- Wassmann, P., Carroll, J., Bellerby, R.G.J., 2008. Carbon flux and ecosystem feedback in the northern Barents Sea in an era of climate change: an introduction. *Deep-Sea Res. II* 55, 2143–2153.
- Zaborska, A., Carroll, J., Papucci, C., Torricelli, L., Carroll, M.L., Walkusz-Miotk, J., Pempkowiak, J., 2008. Recent sediment accumulation rates for the western margin of the Barents Sea. *Deep-Sea Res. II* 55, 2352–2360.